Charge density waves and metal-insulator transition in $TaSe_2$

Benrui Huang,[1,3] Lin Wang,[2] Ni Ma,[1,3] Kaiyi Li,[4] Jingpeng Song,[1,3] Gang Chen,[2] and Ang Li[1,3,*]

[1]*State Key Laboratory of Functional Materials for Informatics, Shanghai Institute of Microsystem and Information Technology, Chinese Academy of Sciences, Shanghai 200050, China*

[2]*State Key Laboratory of Infrared Physics, Shanghai Institute of Technical Physics, Chinese Academy of Sciences, Shanghai 200083, China*

[3]*Center of Materials Science and Optoelectronics Engineering, University of Chinese Academy of Sciences, Beijing 100049, China*

[4]*School of Physical Science and Technology, ShanghaiTech University, Shanghai 201210, China*

(Received 9 July 2021; revised 27 August 2021; accepted 9 September 2021; published 20 September 2021)

Using scanning tunneling microscopy/spectroscopy (STM/STS), we investigate the local atomic and electronic structure of the archetype charge density wave (CDW) system $TaSe_2$. Two structural phases with distinct CDW orders, namely 3×3-$2H$ and $\sqrt{13}\times\sqrt{13}$-$1T$ phases, coexist at low temperatures and an intermediate phase is discovered around the phase boundaries demonstrating energy-dependent $2H$ and $1T$ electronic wave-function textures. The existence of such an intermediate state and its dual electronic appearance indicate that the $2H$-$1T$ transition is not instantaneous. Along with the gradual recovery of $\sqrt{13}\times\sqrt{13}$-$1T$ lattice distortions towards the $2H$ phase, an insulator-metal transition occurs as evidenced by the collapse of the Mott insulating gap. Our results provide a direct visualization of the strong link between the Mott insulating state and the local lattice distortions.

DOI: 10.1103/PhysRevB.104.115136

I. INTRODUCTION

The Mott insulating state is characterized by a strong electron-electron Coulomb interaction that opens an excitation gap in a partially filled electronic band. It can host various quantum phenomena such as high-temperature superconductivity [1,2] and colossal magnetoresistance [3,4]. Transition metal dichalcogenides (TMDs) provide another feasible platform for the study of Mott correlation and related electronic instabilities. Two examples are the bulk $1T$-TaS_2 and the surface of $1T$-$TaSe_2$ hosting a Mott insulating ground state [5–8]. Intriguingly, a Mott insulator-metal transition can be induced by pressure [9], photoexcitation [10,11], electric current [12–14], pulse voltage [15,16], and chemical substitution [17–19]. The nature of Mott insulation and a metal-insulator transition (MIT) is closely related to the prominent charge density wave (CDW) orders in TMDs but the physical mechanisms behind them remain controversial.

TMDs are a class of layered van der Waals materials whose crystal structures can be classified as, depending on the local coordination of chalcogen atoms around the central transition metal, $1H$ (trigonal-prismatic), $1T$ (octahedral), and $1T'$ (distorted octahedral with lateral displacement) configurations [20,21]. $1T$ and $2H$ are the most commonly observed bulk phases ($2H$ refers to the AB stacking of $1H$ layers [22]), while the $4H_b$ phase consists of alternating $1H$ and $1T$ layers [23,24] (here the term "layer" is defined as a chalcogen–transition metal–chalcogen triatomic layer unit). In addition to the rich structural phases, complex CDW orders have been observed in TMDs, each being characterized with distinctive lattice distortions. As an archetype CDW material, $2H$-$TaSe_2$ undergoes an incommensurate CDW (ICCDW) transition at 120 K, followed by a transition towards commensurate CDW (CCDW) at 90 K [25]. $2H$-$TaSe_2$ remains metallic all along and a 3×3 lattice distortion is developed in the low-temperature CCDW phase. Similarly in $1T$-$TaSe_2$, ICCDW and CCDW are established below 600 and 473 K successively, the latter demonstrating a $\sqrt{13}\times\sqrt{13}$ star-of-David lattice distortion [24]. In addition, the Mott insulating phase sets in below 260 K in $1T$-$TaSe_2$ [7,8]. It is widely believed that the MIT is driven by the narrowing of a Ta $5d$-electron band as a result of the atomic displacement in the $\sqrt{13}\times\sqrt{13}$ CDW phase [7]. However, interlayer coupling (CDW stacking order) has also been proposed both theoretically and experimentally to govern the MIT [16,26]. Therefore, it is crucial to track the evolution of the electronic state with the long-range CDW order.

Here, we report a low-temperature scanning tunneling microscopy/spectroscopy (STM/STS) study of the atomic and electronic structure of $TaSe_2$. In addition to the spatial coexistence of $2H$ and $1T$ CCDW phases ($2H$ and $1T$ for short; when referring to CDW order, they denote the 3×3 CCDW in $2H$-$TaSe_2$ and $\sqrt{13}\times\sqrt{13}$ CCDW in $1T$-$TaSe_2$ respectively for convenience), we found an intermediate phase carrying both $2H$ and $1T$ textures in the local density of states (LDOS). The existence of such an intermediate state and its dual electronic appearance reflect the noninstantaneous nature of the $2H$-$1T$ CDW transition where slow lattice dynamics must be involved. Concomitant with the progressive recovery of $\sqrt{13}\times\sqrt{13}$-$1T$ lattice distortion, an insulator-metal transition occurs as evidenced by the collapse of the Mott insulating gap. Our results highlight the primary connection between the Mott insulating state and the $1T$ lattice distortion. A lattice

*angli@mail.sim.ac.cn

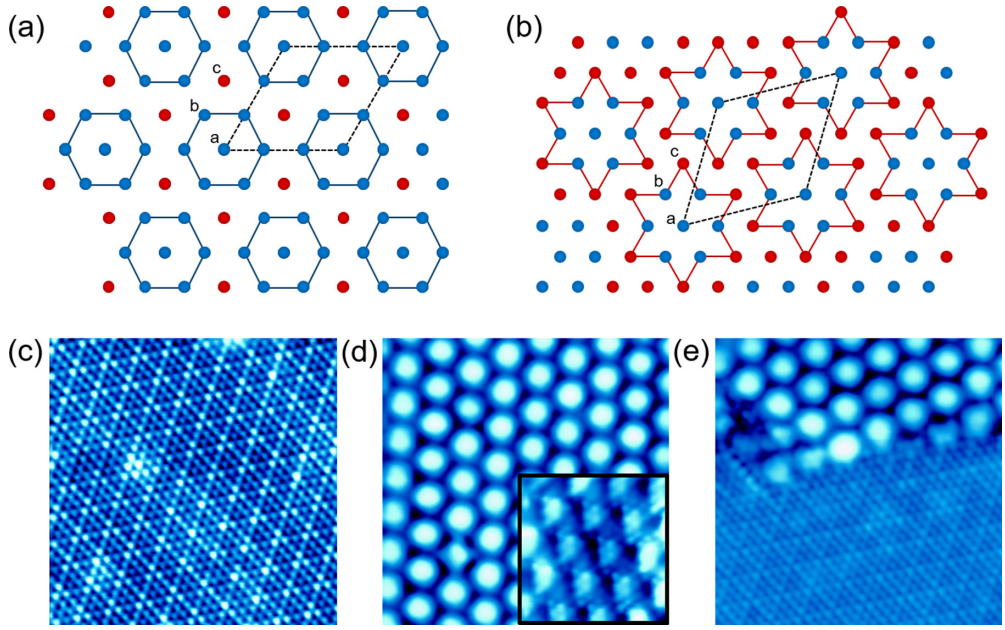

FIG. 1. In-plane atomic structure for the Ta layer in (a) $2H$- and (b) $1T$-$TaSe_2$. For clarity, the upper and lower layers of Se atoms are not shown. Dashed rhombuses represent the unit cells of a 3×3 and $\sqrt{13}\times\sqrt{13}$ CDW superlattice. Solid hexagons (blue) and stars of David (red) highlight the local lattice distortion (contraction) of each CDW phase. The letters a, b, and c mark the central, six nearest-neighbor, and six next-nearest-neighbor Ta atoms, respectively. (c) Topographic image of the $2H$ CDW phase (bias voltage $V = 200$ mV, tunneling current $I = 500$ pA, 10×10 nm^2). (d) Topographic image for the $1T$ CDW phase ($V = -100$ mV, $I = 100$ pA, 10×10 nm^2). The inset shows the atomic resolution ($V = 15$ mV, $I = 100$ pA, 5×5 nm^2). (e) A 10×10 nm^2 area showing the coexisting $2H$, $1T$ phase, and phase boundary ($V = -100$ mV, $I = 100$ pA).

degree of freedom plays an important role in the CDW orders as well as the formation of strong electron correlation.

II. METHODS

Single crystalline $TaSe_2$ samples were grown via the ambient-pressure chemical vapor deposition (CVD) method [27]. The STM/STS experiments were carried out in ultrahigh vacuum at $T = 4.5$ K. Samples were cleaved *in situ* at about 77 K and quickly transferred to the cold microscope head. The STM tips were prepared from polycrystalline tungsten wires by electrochemical etching and calibrated on a clean Cu(111) surface before all STM measurements. The topographic images were acquired in the constant current mode with bias voltage applied to the sample. The spectroscopic data (differential conductance dI/dV) were recorded with a standard lock-in technique.

III. RESULTS AND DISCUSSIONS

The atomic layouts of Ta layers in $2H$ and $1T$ CDW phases are schematically drawn in Figs. 1(a) and 1(b). For the $2H$ CDW, six nearest-neighbor Ta atoms [labeled b in Fig. 1(a)] distort around the central Ta atom (labeled a) to form a 3×3 superlattice. Distinctly, the $1T$ phase is characterized by the star-of-David pattern, which involves six nearest-neighbor (b) and six next-nearest-neighbor Ta atoms (c) shrinking towards the central Ta atom (a) to form a $\sqrt{13}\times\sqrt{13}$ superstructure. In any case, the structural distortion and charge modulation in the Ta layer are expected to be reflected in the Se layer as well, which is the surface exposed after cleaving. Indeed, characteristic $2H$ and $1T$ CDW orders are resolved experimentally with atomic resolution as shown in Figs. 1(c) and 1(d). The bright balls in Fig. 1(d), for instance, represent the star-of-David pattern in the $1T$ phase, each involving 13 Ta atoms underneath. The $2H$ and $1T$ phases coexist in $TaSe_2$ separated by the phase boundaries [Fig. 1(e)]. It is consistent with the density functional theory (DFT) calculation [28] which shows the energy difference between $1T$ and $2H$ polymorphs in $TaSe_2$ is fairly small.

In addition, a third type of topography appears near the $2H$ and $1T$ coexisting area. In contrast to that of an intrinsic $2H$ or $1T$ phase, it demonstratesan apparent bias dependence as shown in Figs. 2(a)–2(h) (there exists a small drift during the scan). To be specific, it shows $1T$ stars under the positive bias voltage but becomes more $2H$-like under the negative bias. The change is reversible and cannot be caused by the pulse voltage (in our experiment, the bias voltage is varied carefully in small steps), electric field (Fig. S1 in Supplemental Material [29], topographic features remain unchanged as the electric field is varied), or joule heating [e.g., tunneling current is kept constant in Figs. 2(c)–2(h)]. Nor is it due to any artificial effects such as a double tip [29]. Similar bias-dependent behaviors have been reported in $1T$-TaS_2 [16,28] and $4H_b$-TaS_2 [30]. It is explained as a $1H$-monolayer stacking on $1T$ layer(s) that the underlying $1T$ phase can be resolved at appropriate energies due to the difference in density of states (DOS). However, unlike TaS_2, the DOS of $1T$ monolayer $TaSe_2$ near the Fermi level is much lower than that of $1H$ [22,31], which means the $1T$-$TaSe_2$ cannot be resolved through the top $1H$-$TaSe_2$ in this energy range. Experimentally, instead, clear $1T$ features are observed

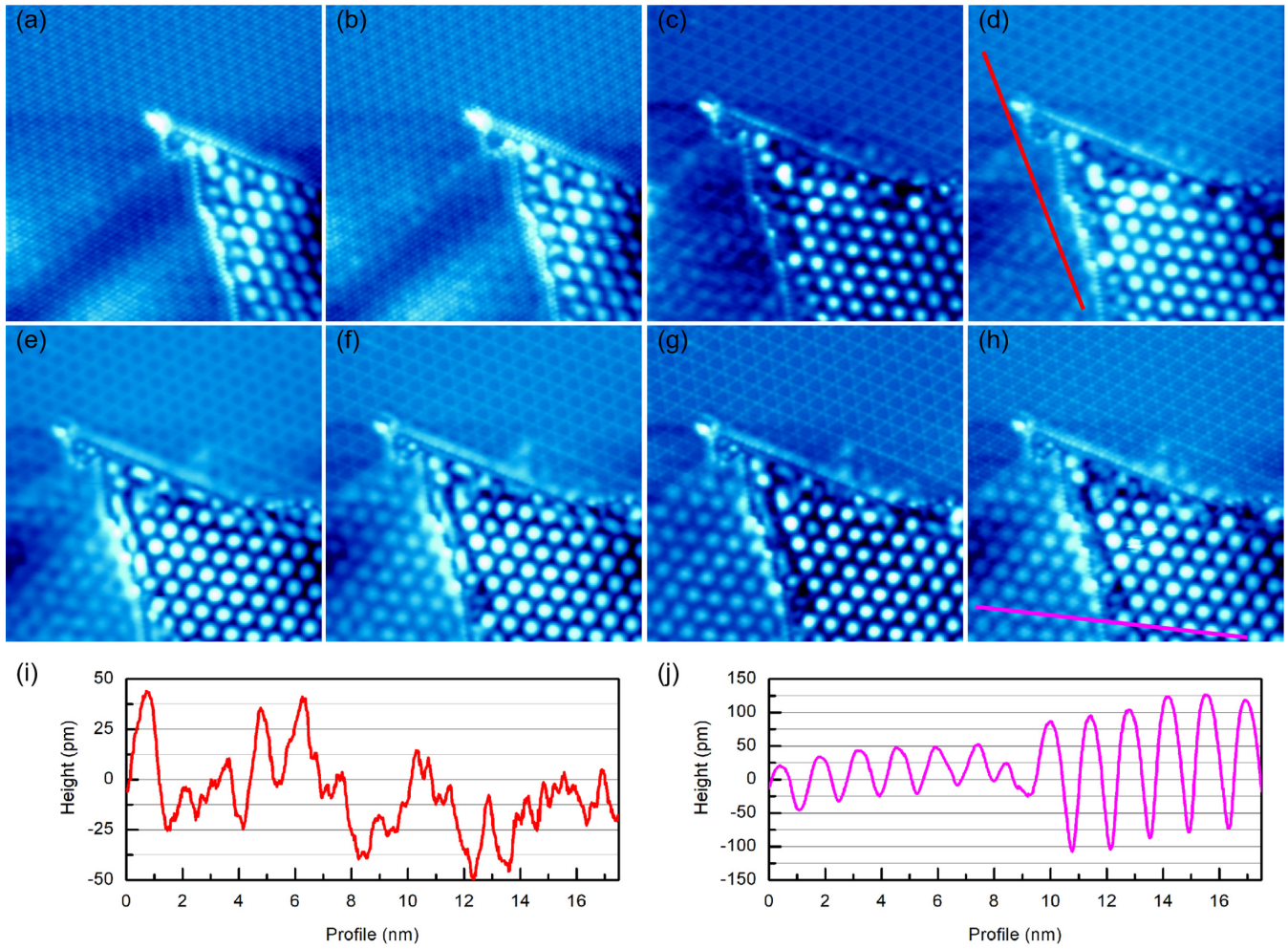

FIG. 2. (a)–(h) Topographic images at different bias voltages (20×20 nm^2). The lower left quarter corresponds to the intermediate phase. Profiles along the red and pink lines in (d) and (h) are shown in (i) and (j) with corresponding color. Scan parameters: (a) $V = -500$ mV, $I = 100$ pA; (b) $V = -300$ mV, $I = 100$ pA; (c) $V = -200$ mV, $I = 500$ pA; (d) $V = -100$ mV, $I = 500$ pA; (e) $V = 500$ mV, $I = 500$ pA; (f) $V = 300$ mV, $I = 500$ pA; (g) $V = 200$ mV, $I = 500$ pA; (h) $V = 100$ mV, $I = 500$ pA.

at ±5 mV as shown in Fig. S2. A further comparison with the $4H_b$ phase is discussed in the Supplemental Material [29].

Moreover, the topographic height difference with an adjacent $2H$ or $1T$ surface is much smaller than the thickness of the $TaSe_2$ monolayer (750 pm) [32]. In general, STM topographies contain contributions from both surface geometry and LDOS. In order to minimize the influence of different LDOS, two line profiles are measured at respective bias voltages referring to the corresponding $1T$ and $2H$ regions [Figs. 2(d) and 2(h)]. When the $2H$ ($1T$) topography dominates, it is compared to the intrinsic $2H$ ($1T$) phase nearby. Both cases show negligible height differences (less than 50 pm) that are one order of magnitude smaller than the thickness of the Se-Ta-Se monolayer. Therefore, the bias dependence of topographies in Fig. 2 does not come from the competition of integrated LDOS from different layers. They reflect the energy-dependent textures of the electronic wave function in the surface of one particular area. As these areas are always found close to the $2H$ and $1T$ phase boundaries, we believe such a "mixed" phase represents an intermediate (precursor) state in the $2H$-$1T$ transition.

In order to further explore the evolution of electronic states as a function of energy, dI/dV mapping containing the $1T$ (upper left corner), intermediate (main), and $2H$ phase (lower right corner) is performed in Figs. 3 and S4. Stars of David in the $1T$ phase reveal orbital textures similar to those reported in TaS_2 [19,31,33]. In the intermediate state, while the $2H$ characters are mainly distributed over the occupied states (negative bias voltage), the $1T$ star pattern can be resolved throughout the entire energy range. The $2H$ spectral weight decreases from high negative bias towards the Fermi level, thus the $1T$ features become dominant above -40 meV. This trend is captured exactly in the topographies that correspond to the integrated LDOS. The existence of such an intermediate state and its dual electronic appearance indicate that the $2H$-$1T$ CDW transition is not instantaneous. In addition to the charge redistribution, slow lattice dynamics must be involved which could be driven by external stimulations (such as the pulse voltage) and remain metastable. Nevertheless, it does not mean the local atomic structure is switching in the intermediate state as we sweep the bias voltage. The atoms should stay at transitional positions between the $1T$ and $2H$

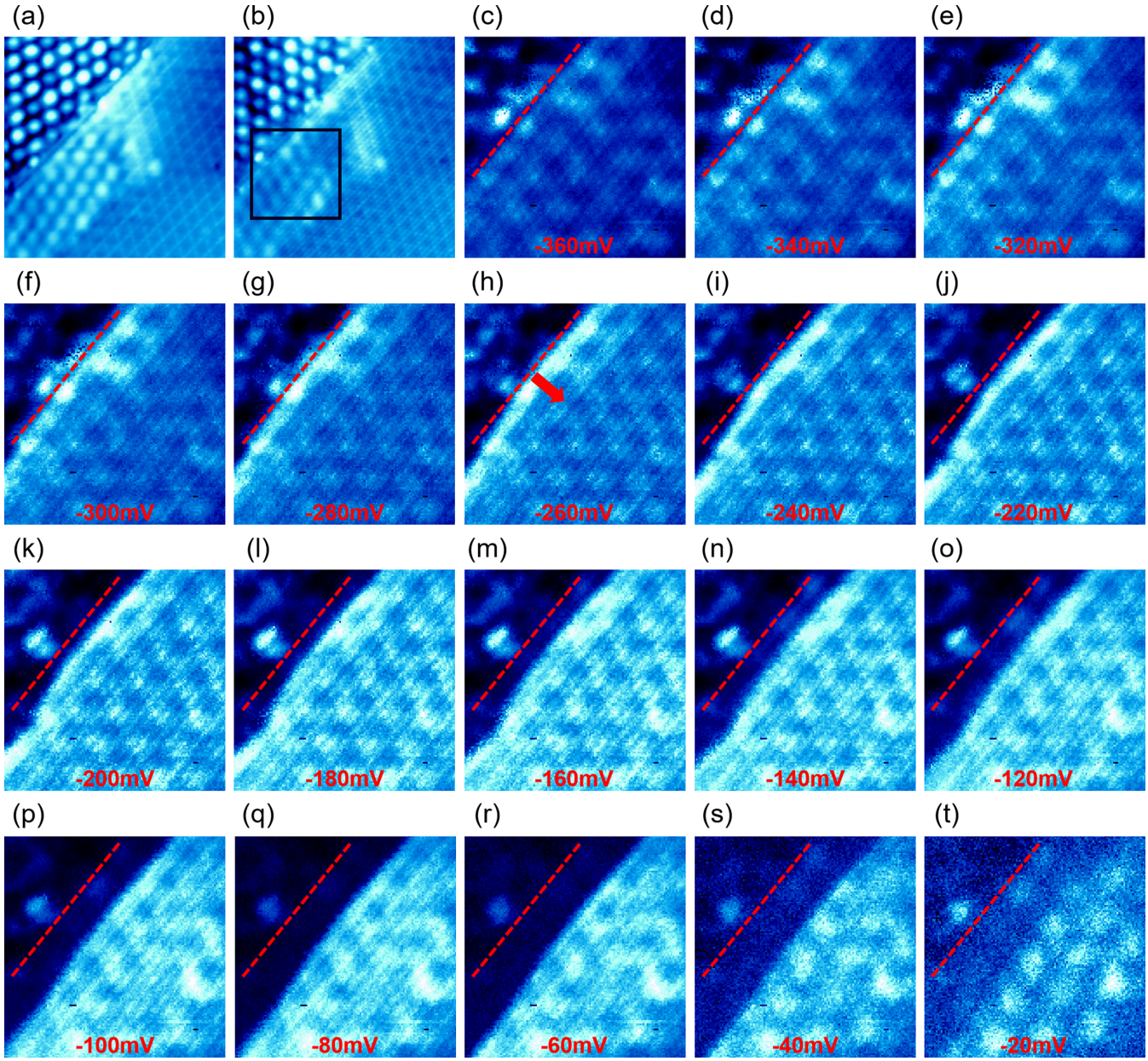

FIG. 3. (a), (b) Topographic images for a junction area of multiple phases [15×15 nm^2, $I = 200$ pA, (a) $V = 400$ mV and (b) -400 mV]. (c)–(t) dI/dV maps acquired within the box in (b). The red dashed lines mark the initial position of frontline and the red arrow in (h) indicates its moving direction (6×6 nm^2, $V = 400$ mV, $I = 100$ pA, lock-in modulation amplitude $\Delta V = 20$ mV at frequency $f = 973$ Hz).

sites. The bias-dependent behavior reveals the energy distribution of $1T$ and $2H$ characters in the electronic wave function during the transition.

As expected, an MIT occurs with the $2H$-$1T$ CDW transition. Figure 4 shows the typical dI/dV spectra for intrinsic $2H$, $1T$, and the intermediate state. A Mott gap is clearly visible in the intrinsic $1T$ phase with two peaks located around -210 and $+220$ meV corresponding to the lower and upper Hubbard bands, respectively [8]. The gap edges shift towards the Fermi level and the in-gap density of states (DOS) is partially recovered in the intermediate state. Eventually, metallicity with finite DOS is restored in the intrinsic $2H$ phase. For comparison, a spectrum in the $1T$ phase close to the phase boundary (PB) (hence neighboring $2H$) is plotted in Fig. 4 as well. It shows similar spectral features as that in the intermediate state.

The progressive transition can be tracked more explicitly in our spectroscopic mapping data. In Figs. 3(c)–3(t), a frontline is observed in the intermediate phase propagating towards the lower right $2H$ corner as the $2H$ features fade away with the decrease of energy (the initial location is marked by a red dashed line). The frontline corresponds to the lower-Hubbard-band maximum in the dI/dV spectrum. Its movement visualizes the shift of the Hubbard band when the $2H$ phase is approached, highlighting the Mott insulator-to-metal transition.

Meanwhile, the $1T$ local lattice distortion (contraction) relaxes as evidenced by the average diameter of the stars of

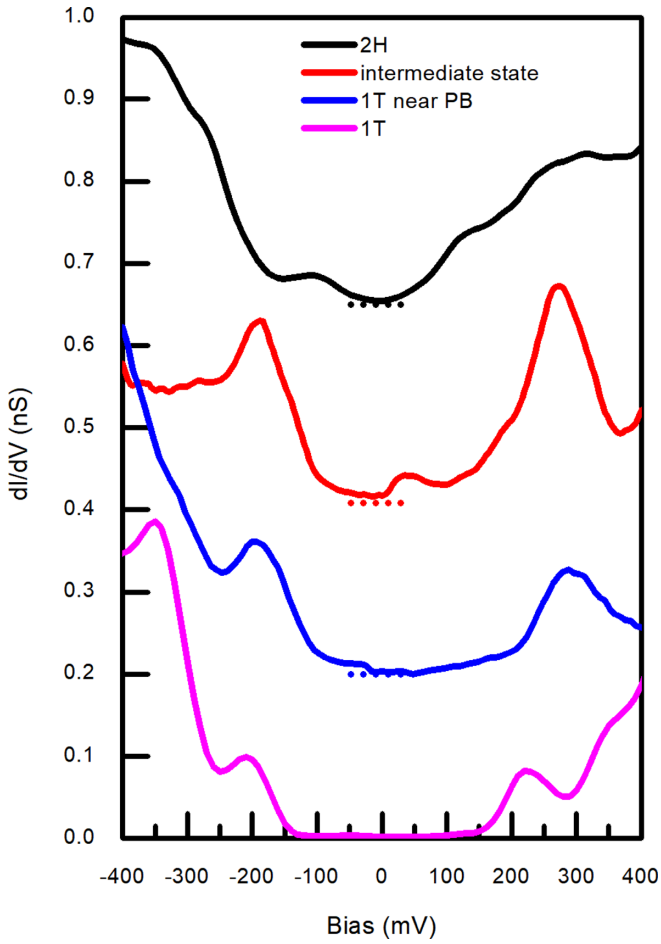

FIG. 4. Typical dI/dV spectra for intrinsic $2H$, $1T$, and intermediate state as well as $1T$ close to the $1T$-$2H$ phase boundaries (PBs) ($V = -400$ mV, $I = 500$ pA, $\Delta V = 8$ mV, $f = 973$ Hz). The spectra are shifted vertically for clarity (the horizontal bars mark $dI/dV = 0$).

David expanding from 1.27 to 1.39 nm (Fig. S5). These results suggest that the Mott insulating state is intimately related to the star-of-David distortion, which has a direct impact on the overlapping and hybridization of Ta d orbitals [7]. Thus the MIT can be effectively described by the one-band Hubbard model. The bandwidth W increases when the lattice distortion is relaxed. As a result, the U/W (U: on-site Coulomb repulsion) decreases. Once reaching a critical value, the Mott insulating state becomes metallic [15].

It was proposed that the vertical stacking order of $1T$ CDW would dictate the ground state in bulk TaS_2 [26]. A similar argument that interlayer coupling weakens the Mott insulation was reported for few-layer $TaSe_2$ films [31]. Here, we can hardly address this issue as no atomic steps were found in this study. Nevertheless, a $1T$ structural configuration is prerequired. We believe the MIT accompanying the $2H$-$1T$ CDW transition is primarily driven by the band tuning in response to the in-plane atomic displacement in the $1T$ CDW state. It is reasonable to conceive that moderate structural modifications as revealed in this study alter the hybridization of d orbitals that eventually change the electronic structure [19]. In line with this scenario, a recent theoretical work demonstrates the Mottness collapse in monolayer $1T$-$TaSe_2$ under pressure without losing the long-range CDW order [34].

IV. CONCLUSIONS

In summary, using scanning tunneling microscopy, we studied the CDW orders and metal-insulator transition in $TaSe_2$ single crystals. In addition to the coexisting $2H$ and $1T$ CDW orders, an intermediate (precursor) phase is identified carrying both $2H$ and $1T$ features in LDOS at representative energies. Such an "adiabatically" accessed intermediate state reveals the noninstantaneous nature of the $2H$-$1T$ CDW transition where relatively slow lattice dynamics should be involved. Concomitant with the progressive recovery of $\sqrt{13}\times\sqrt{13}$ lattice distortion from $1T$ towards $2H$, an insulator-metal transition occurs as evidenced by the collapse of the Mott insulating gap. Our results emphasize the close connection between the Mott insulating state and the $1T$ local lattice distortion.

ACKNOWLEDGMENTS

This work was supported by the National Natural Science Foundation of China (NSFC) (Grants No. 11227902 and No. 62075230), State Key Program for Basic Research of China (Grant No. 2018YFA0306204), Natural Science Foundation of Shanghai (Grants No. 18ZR1447300 and No. 19ZR1465400), and Shanghai Municipal Science and Technology Major Project (Grant No. 2019SHZDZX01).

[1] P. A. Lee, N. Nagaosa, and X.-G. Wen, Rev. Mod. Phys. **78**, 17 (2006).
[2] G. Baskaran, Phys. Rev. Lett. **90**, 197007 (2003).
[3] M. Zhu, J. Peng, T. Zou, K. Prokes, S. D. Mahanti, T. Hong, Z. Q. Mao, G. Q. Liu, and X. Ke, Phys. Rev. Lett. **116**, 216401 (2016).
[4] E. Janod, E. Dorolti, B. Corraze, V. Guiot, S. Salmon, V. Pop, F. Christien, and L. Cario, Chem. Mater. **27**, 4398 (2015).
[5] J. Wilson and A. Yoffe, Adv. Phys. **18**, 193 (1969).
[6] P. Fazekas and E. Tosatti, Philos. Mag. B **39**, 229 (1979).
[7] L. Perfetti, A. Georges, S. Florens, S. Biermann, S. Mitrovic, H. Berger, Y. Tomm, H. Höchst, and M. Grioni, Phys. Rev. Lett. **90**, 166401 (2003).
[8] S. Colonna, F. Ronci, A. Cricenti, L. Perfetti, H. Berger, and M. Grioni, Phys. Rev. Lett. **94**, 036405 (2005).
[9] B. Sipos, A. F. Kusmartseva, A. Akrap, H. Berger, L. Forró, and E. Tutiš, Nat. Mater. **7**, 960 (2008).
[10] S. Hellmann, M. Beye, C. Sohrt, T. Rohwer, F. Sorgenfrei, H. Redlin, M. Kalläne, M. Marczynski-Bühlow, F. Hennies, M. Bauer, A. Föhlisch, L. Kipp, W. Wurth, and K. Rossnagel, Phys. Rev. Lett. **105**, 187401 (2010).

[11] L. Stojchevska, I. Vaskivskyi, T. Mertelj, P. Kusar, D. Svetin, S. Brazovskii, and D. Mihailovic, Science **344**, 177 (2014).
[12] I. Vaskivskyi, I. A. Mihailovic, S. Brazovskii, J. Gospodaric, T. Mertelj, D. Svetin, P. Sutar, and D. Mihailovic, Nat. Commun. **7**, 11442 (2016).
[13] M. J. Hollander, Y. Liu, W.-J. Lu, L.-J. Li, Y.-P. Sun, J. A. Robinson, and S. Datta, Nano Lett. **15**, 1861 (2015).
[14] M. Yoshida, R. Suzuki, Y. Zhang, M. Nakano, and Y. Iwasa, Sci. Adv. **1**, (2015) doi:10.1126/sciadv.1500606.
[15] D. Cho, S. Cheon, K.-S. Kim, S.-H. Lee, Y.-H. Cho, S.-W. Cheong, and H. W. Yeom, Nat. Commun. **7**, 10453 (2016).
[16] L. Ma, C. Ye, Y. Yu, X. F. Lu, X. Niu, S. Kim, D. Feng, D. Tománek, Y.-W. Son, X. H. Chen, and Y. Zhang, Nat. Commun. **7**, 10956 (2016).
[17] R. Ang, Y. Tanaka, E. Ieki, K. Nakayama, T. Sato, L. J. Li, W. J. Lu, Y. P. Sun, and T. Takahashi, Phys. Rev. Lett. **109**, 176403 (2012).
[18] R. Ang, Y. Miyata, E. Ieki, K. Nakayama, T. Sato, Y. Liu, W. J. Lu, Y. P. Sun, and T. Takahashi, Phys. Rev. B **88**, 115145 (2013).
[19] S. Qiao, X. Li, N. Wang, W. Ruan, C. Ye, P. Cai, Z. Hao, H. Yao, X. Chen, J. Wu, Y. Wang, and Z. Liu, Phys. Rev. X **7**, 041054 (2017).
[20] G. Eda, T. Fujita, H. Yamaguchi, D. Voiry, M. Chen, and M. Chhowalla, ACS Nano **6**, 7311 (2012).
[21] A. L. Friedman, A. T. Hanbicki, F. K. Perkins, G. G. Jernigan, J. C. Culbertson, and P. M. Campbell, Sci. Rep. **7**, 3836 (2017).
[22] Y. Nakata, T. Yoshizawa, K. Sugawara, Y. Umemoto, T. Takahashi, and T. Sato, ACS Appl. Nano Mater. **1**, 1456 (2018).
[23] I. Ekvall, J.-J. Kim, and H. Olin, Phys. Rev. B **55**, 6758 (1997).
[24] J. Wilson, F. D. Salvo, and S. Mahajan, Adv. Phys. **24**, 117 (1975).
[25] D. E. Moncton, J. D. Axe, and F. J. DiSalvo, Phys. Rev. Lett. **34**, 734 (1975).
[26] S.-H. Lee, J. S. Goh, and D. Cho, Phys. Rev. Lett. **122**, 106404 (2019).
[27] L. Wang, J. Wang, C. Liu, H. Xu, A. Li, D. Wei, Y. Liu, G. Chen, X. Chen, and W. Lu, Adv. Funct. Mater. **29**, 1905057 (2019).
[28] Z. Wang, Y.-Y. Sun, I. Abdelwahab, L. Cao, W. Yu, H. Ju, J. Zhu, W. Fu, L. Chu, H. Xu, and K. P. Loh, ACS Nano **12**, 12619 (2018).
[29] See Supplemental Material at http://link.aps.org/supplemental/10.1103/PhysRevB.104.115136 for (1) the independence of intermediate state on electric field, (2) the $1T$ characters that can be resolved near Fermi energy in the intermediate state, (3) comparison with $4H_b$ phase, (4) full data set of dI/dV map, (5) the lattice distortion of star-of-David in $1T$ CDW phase, and (6) discussions about the possibility of a double tip effect.
[30] C. Wen, J. Gao, Y. Xie, Q. Zhang, P. Kong, J. Wang, Y. Jiang, X. Luo, J. Li, W. Lu, Y.-P. Sun, and S. Yan, Phys. Rev. Lett. **126**, 256402 (2021).
[31] Y. Chen, W. Ruan, M. Wu, S. Tang, H. Ryu, H.-Z. Tsai, R. L. Lee, S. Kahn, F. Liou, C. Jia, O. R. Albertini, H. Xiong, T. Jia, Z. Liu, J. A. Sobota, A. Y. Liu, J. E. Moore, Z.-X. Shen, S. G. Louie, S.-K. Mo *et al.*, Nat. Phys. **16**, 218 (2020).
[32] P. Hajiyev, C. Cong, C. Qiu, and T. Yu, Sci. Rep. **3**, 2593 (2013).
[33] D. Cho, Y.-H. Cho, S.-W. Cheong, K.-S. Kim, and H. W. Yeom, Phys. Rev. B **92**, 085132 (2015).
[34] K. Zhang, C. Si, C.-S. Lian, J. Zhou, and Z. Sun, J. Mater. Chem. C **8**, 9742 (2020).